PCCP

PAPER

View Article Online
View Journal | View Issue

Cite this: *Phys. Chem. Chem. Phys.*, 2025, **27**, 18907

Kinetics of the reaction of CF_3CHO with OH between 204 K and 361 K

Fabienne Baumann, * Christin Fernholz, Jos Lelieveld and John N. Crowley *

Trifluoroacetaldehyde (CF_3CHO) is formed in the atmosphere by the oxidation of a number of fluorinated, organic compounds of anthropogenic origin. The reaction of CF_3CHO with the OH radical is a potential source of atmospheric trifluoroacetic acid (TFA) which is a highly persistent, water-soluble compound that may accumulate in aquatic ecosystems and for which uncertainty about its sources, fate, and potential ecological impact persists. In light of growing concerns about the impact of TFA, we present the first study of the temperature dependence of the rate coefficient for the title reaction over the atmospherically relevant temperature range of 204 K to 361 K. Rate coefficients were determined using pulsed laser photolysis–pulsed laser induced fluorescence (PLP–PLIF) and direct concentration measurements *via* Fourier Transform Infrared (FTIR) spectroscopy, as well as relative rate experiments in an atmospheric simulation chamber using ethane (C_2H_6) as a reference compound. The rate coefficient (k_1) obtained with PLP–PLIF at room temperature is $(5.8 \pm 0.5) \times 10^{-13}$ cm^3 molecule^{-1} s^{-1}. The temperature dependence is described by the expression $k_1(T) = (3.8 \pm 0.2) \times 10^{-13} \times (T/300)^2 \times \exp[(131 \pm 16)/T]$. The relative-rate experiments showed that the rate coefficient obtained can be significantly biased by reactions of the CF_3O radical with CF_3CHO and/or C_2H_6 and also reactions of CF_3CHO with HO_2. Based on the expression of k_1 given above, the lifetime of CF_3CHO with respect to reaction with the OH radical varies from 22 days at the surface ($T \sim 300$ K) to 30 days in the upper troposphere ($T \sim 220$ K).

Received 28th July 2025,
Accepted 18th August 2025

DOI: 10.1039/d5cp02871j

rsc.li/pccp

1. Introduction

Fluorinated chemicals are produced at a worldwide annual rate of multiple million tons, with a rising trend. Owing to their chemical stability and unique physicochemical properties,[8] they are widely used as refrigerants, propellants, specialty solvents, and high-performance lubricants. It is estimated that ~20% of marketed drugs and ~50% of agrichemicals contain at least one F-atom underlining their importance.[9,10] The generation and usage of fluorinated trace gases including hydrochlorofluorocarbons (HCFCs), hydrofluorocarbons (HFCs), fluorotelomer alcohols and hydrofluoroolefins (HFOs)[11–13] results in their release to the atmosphere where they may undergo chemical transformation. While HCFCs and HFCs are long-lived (up to decades) and are transported to the stratosphere, HFOs have lifetimes of the order of days to weeks and are degraded in the lower atmosphere (troposphere). HFOs are of topical interest as they are gaining importance as replacements for traditional refrigerants such as chlorofluorocarbons (CFCs) and hydrofluorocarbons (HFCs)[14,15] and are now widely used in a variety of industrial applications, including refrigerants, foam blowing agents and propellants in medical devices.[16–18]

Fluorinated chemicals have come under scrutiny owing to their potential risk to the environment as greenhouse gases or precursors to toxic and persistent chemicals. CF_3CHO, the object of this study, is one of the products that can result from the breakdown of some fluorinated chemicals in the atmosphere.

The atmospheric degradation of CF_3CHO proceeds *via* both photolysis and reaction with OH radicals. Based on the available literature, photolysis is expected to contribute ~80% and reaction with OH ~20%.[19] However, there is considerable uncertainty associated with the relative contribution of these loss pathways at *e.g.* different altitudes, as temperature-dependent rate coefficients for (R1) or temperature dependent quantum yields for (R2) have not been published (IUPAC, 2025).[5] The reaction with OH is thought to proceed entirely *via* abstraction of the aldehydic H-atom to generate the trifluoro acetyl radical (CF_3CO) as written in (R1). The predominant products of photodissociation at actinic wavelengths ($\lambda >$ 300 nm) are CF_3 and HCO (R2).

$$CF_3CHO + OH \rightarrow CF_3CO + H_2O \quad (R1)$$

$$CF_3CHO + h\nu \rightarrow CF_3 + HCO \quad (R2)$$

Max-Planck-Institute for Chemistry, Division of Atmospheric Chemistry, 55128 Mainz, Germany. E-mail: fabienne.baumann@mpic.de, john.crowley@mpic.de

The CF_3CO product of (R1), will react with O_2 in air to form the $CF_3C(O)O_2$ radical (R3), which, *via* subsequent reaction with atmospheric peroxy radicals or reactive nitrogen trace-gases represents a pathway to the formation of stable and semi-stable trace-gases such as $CF_3C(O)OH$ (TFA, (R4a)), $CF_3C(O)OOH$ (trifluoroperacetic acid, (R4b)) and $CF_3C(O)O_2NO_2$ (trifluoroperoxyacetyl nitric anhydride, FPAN, (R5)).[5]

$$CF_3CO + O_2 + M \rightarrow CF_3C(O)O_2 + M \quad (R3)$$

$$CF_3C(O)O_2 + HO_2 \rightarrow CF_3C(O)OH + O_3 \quad (R4a)$$

$$\rightarrow CF_3C(O)OOH + O_2 \quad (R4b)$$

$$\rightarrow CF_3CO_2 + O_2 + OH \quad (R4c)$$

$$CF_3C(O)O_2 + NO_2 + M \rightarrow CF_3C(O)O_2NO_2 + M \quad (R5)$$

Thus, while the photolysis of CF_3CHO leads to radical fragments that further degrade to *e.g.* CO and F_2CO, reaction with OH maintains the C-2 chain and can thus result in the formation of TFA which is a highly persistent, water-soluble compound that is primarily removed from the atmosphere through wet deposition.[20] TFA accumulates in aquatic ecosystems, particularly in oceans and terminal basins, with no known significant degradation pathway.[6] Although current and predicted environmental concentrations are well below toxic thresholds for aquatic life, debates and uncertainties about the sources, fate, and potential ecological impact of TFA persist.[7] The formation of FPAN in (R5) may also represent a chemical pathway to TFA *via* hydrolysis on aqueous hydrometeors or wet-surfaces or even *via* reaction with water vapour.[21]

Several experimental studies of the reaction of CF_3CHO with the OH radical have been published and these have been summarised and evaluated by the IUPAC panel which, in the absence of published, temperature-dependent rate coefficients, makes a recommendation for the rate coefficient at room temperature only with $k_1 = 5.5 \times 10^{-13}$ cm^3 molecule^{-1} s^{-1} at 298 K.[5] This number is reported to be associated with large uncertainty (58%), reflecting the scatter in individual determinations of k_1. Rate coefficients derived using absolute methods vary from 1.1×10^{-12} cm^3 molecule^{-1} s^{-1} (Dóbé *et al.* 1989) to 6.5×10^{-13} cm^3 molecule^{-1} s^{-1} (Scollard *et al.* 1993).[1,2] Relative rate studies also report very different rate coefficients with values of 4.4×10^{-13} cm^3 molecule^{-1} s^{-1} (Scollard *et al.* 1993), 4.8×10^{-13} cm^3 molecule^{-1} s^{-1} (Sellevåg 2004), 6.15×10^{-13} cm^3 molecule^{-1} s^{-1} and 6.93×10^{-13} cm^3 molecule^{-1} s^{-1} (Sulbaek-Andersen 2004).[2,3,22] These studies are discussed in detail in Section 3.2 where we compare them with our results.

For the equivalent non-fluorinated acetaldehyde (CH_3CHO) a negative temperature dependence for reaction with OH has been reported by Sivakumaran *et al.* 2003 and IUPAC over the temperature range 200–380 K.[5,23] Literature studies have shown that the rate coefficient for OH with CH_3CHO is orders of magnitude larger than that for OH + CF_3CHO indicating a strong effect of the fluorine atoms on the reactions potential energy surface and thus its temperature dependence. The lack of published, temperature-dependent kinetic data for OH + CF_3CHO thus makes prediction of its lifetime at various altitudes in the troposphere (where temperatures may vary between ~300 and 230 K) precarious and precludes accurate assessment of the lifetime of CF_3CHO and its potential to lead to TFA formation.

The objective of this research is to experimentally determine the temperature-dependent rate coefficient for the reaction of CF_3CHO with OH. To achieve this, we have used pulsed laser photolysis coupled with pulsed laser-induced fluorescence (PLP–PLIF) and online gas-phase FTIR measurements of reactant concentrations, which enable precise determination of rate coefficients across a large temperature range. Additionally, we conducted room-temperature relative-rate experiments in a photolytic reactor with *in situ* FTIR analysis (RR-FTIR).

2. Experimental

Absolute, temperature-dependent rate coefficients, $k_1(T)$, for the title reaction were obtained using pulsed laser photolytic (PLP) generation of OH coupled to pulsed laser induced fluorescence (PLIF) detection with $[CF_3CHO] \gg [OH]$ (pseudo-first-order conditions). The concentration of CF_3CHO was measured *in situ via* Fourier-transform infra-red absorption (FTIR) spectroscopy. In further, relative-rate experiments using a photolytic chamber with FTIR absorption spectroscopy (RR-FTIR), the room temperature (298 ± 2 K) rate coefficient was measured using C_2H_6 as reference reactant. The experimental setups are briefly described below; further details for the PLP–PLIF and RR-FTIR set-ups are found in Wollenhaupt *et al.* 2000 and Groß *et al.* 2014 (PLP–PLIF) and in Crowley *et al.* 1999 and Berasategui *et al.* 2020 (RR-FTIR).[24–27]

2.1. PLP–PLIF experiments

Experiments were carried out in a double-jacketed quartz reactor (volume ~500 cm^3) thermostatted by circulating ethanol (204 K to 300 K) or water (300 K to 364 K). The reactor is equipped with a K-type thermocouple, which was used to probe the temperature in the centre of the reactor (where the photolysis and excitation laser pulses overlap) before each experiment. The pressure in the reactor and FTIR-absorption cell (see below) was measured using 100 and 1000 Torr capacitance manometers. Gas flows were set up so that a linear velocity of ~70 cm s^{-1} was achieved, ensuring complete gas exchange for each photolysis pulse (10 Hz), preventing the accumulation of products. Gases were pre-mixed in a glass manifold before flowing into the reactor. A distance of ~15 cm between the reactor inlet and the photolysis zone ensured a thermal equilibration with the reactor walls.

2.1.1. Generation of OH. Pulsed radiation for the *in situ* OH-radical generation from a suitable gas-phase precursor (see below) was provided by a KrF excimer laser (COMPex pro 201F, Coherent), which delivered pulses (~20 ns) at 248 nm perpendicular to the gas flow direction. The laser fluence was measured with a Joule–meter positioned behind the exit window of the reactor and, based on the precursor absorption

cross-section and quantum yield at 248 nm, was used to calculate approximate, initial OH concentrations. A total of four schemes ((R6), (R7), (R8) + (R9), (R8) + (R10)) for generating OH were tested.

$$H_2O_2 + h\nu\ (248\ nm) \rightarrow 2\ OH \quad (R6)$$

$$HNO_3 + h\nu\ (248\ nm) \rightarrow OH + NO_2 \quad (R7)$$

$$O_3 + h\nu\ (248\ nm) \rightarrow O(^1D) + O_2 \quad (R8)$$

$$O(^1D) + H_2O \rightarrow 2\ OH \quad (R9)$$

$$O(^1D) + CH_4 \rightarrow OH + CH_3 \quad (R10)$$

Apart from photolysis of H_2O_2 all other schemes suffered from problems related to secondary chemistry or (for HNO_3) surface reaction with CF_3CHO. These issues are highlighted and discussed in the SI. All the PLP–PLIF rate coefficients we report were thus obtained using H_2O_2 as OH source, whereby typical H_2O_2 concentrations of $\sim 5 \times 10^{14}$ molecule cm^{-3} resulted in initial OH concentrations of (1–5) $\times 10^{10}$ molecule cm^{-3}.

2.1.2. Detection of OH and CF_3CHO. OH radicals were excited ($A^2\Sigma(\nu = 1) \leftarrow X^2\Pi\ (\nu = 0)$ transition) at $\sim$282 nm using a YAG-pumped dye laser (Quantel Brilliant B, Lambda Physik Scanmate). The subsequent OH fluorescence was detected using a photomultiplier screened by an interference filter (309 $\pm$ 5 nm). The triggering of the photolysis and probe lasers was controlled by a digital delay generator. Transient OH profiles consisting of 20 pre-excimer pulses and 50 post-excimer pulses were obtained by accumulating the fluorescence signal using a boxcar averager. To achieve an improved signal-to-noise ratio, $\sim$20 OH profiles were accumulated for the derivation of decay kinetics.

The CF_3CHO concentration was monitored by its infra-red absorption in a 45 cm long cell coupled to a FTIR spectrometer (Bruker-Vector 22 with an external, L_{N2}-cooled MCT detector). The absorption cell could be located either upstream or downstream of the reactor. Infrared absorption spectra were recorded with a resolution of 1 cm^{-1} by coaddition of 64 interferograms (background: 128 interferograms) and phase-corrected and Boxcar-apodized (Mertz) with a zero-filling factor of 4. The measured CF_3CHO IR-absorbance was converted to a concentration by spectral deconvolution/fitting to a calibrated, CF_3CHO reference spectrum as well as other relevant absorbing species. There were no strong, unassigned bands in the spectrum and later we set upper limits to the concentrations of IR-absorbing impurities such as C_2H_4. The statistical uncertainty in the CF_3CHO concentration was generally $<$1% and always $<$3%. The CF_3CHO reference spectrum was obtained relative to the well-known UV-absorption spectrum of CF_3CHO by simultaneously recording optical density between 250 and 400 nm and absorbance in the 44 cm FTIR cell. For this purpose, the UV-absorption of CF_3CHO was measured in a multipass absorption cell with 880 cm optical path-length coupled to a UV-vis spectrometer with CCD-camera (Andor DU420A-OE).

The very good agreement in the absorption cross-section of CF_3CHO at λ_{max} = 300 nm between several studies (IUPAC: 3.06 $\times 10^{-20}$, Hashikawa 2006: 3.1 $\times 10^{-20}$, Chiappero 2006: 2.92 $\times 10^{-20}$, Meller 1993: 3.0 $\times 10^{-20}$, Sellevag 2004: 3.17 $\times 10^{-20}$ in cm^2 molecule^{-1}) indicate that the uncertainty associated with the concentrations obtained in this manner (and thus the IR-cross-sections for CF_3CHO) are $<$5%.[3,5,28,29] Cross-sections obtained in independent experiments in which the IR absorption of CF_3CHO was determined using a short absorption cell (10 cm, with the CF_3CHO taken from the headspace of the pure liquid) were used to derive integrated band strengths that agreed to within 3% with those obtained when concentrations were derived by UV-absorption. These results are presented in detail in the SI.

2.2. Relative rate experiments, RR-FTIR

The relative rate experiments were carried out in a 44.39 L cylindrical quartz chamber equipped with *in situ*, infra-red analysis of CF_3CHO and the reference reactants. The same FTIR spectrometer was used as described in the PLP–PLIF experiments, in this case coupled to an internal, white-type multi pass mirror system resulting in an infra-red optical pathlength of 38.4 m. Infrared absorption spectra (600–3600 cm^{-1}) were recorded at 1 cm^{-1} resolution by coaddition of between 64 and 128 interferograms.

Experiments were carried out on static samples at room temperature and a pressure of around 750 Torr using synthetic air or N_2 as bath gases. Gases (C_2H_6, CF_3CHO, H_2 and O_3) were sequentially dosed *via* a glass vacuum line and flushed into the chamber with bath gas. The pressures in the chamber and the vacuum line were measured using capacitance manometers (reactor: 1000 mbar, vacuum line: 1000 mbar, 100 Torr, 10 Torr).

Photochemical OH generation was initiated by the photolysis of O_3 with eight radially-mounted, low-pressure Hg lamps providing a homogeneous light flux ($\sim$253.65 nm) in the chamber. $O(^1D)$ was converted to OH *via* its reaction with H_2 as described previously.[27,30]

$$O_3 + h\nu\ (253.65\ nm) \rightarrow O(^1D_2) + O_2 \quad (R11)$$

$$O(^1D_2) + H_2 \rightarrow OH + H \quad (R12)$$

$$H + O_2 + M \rightarrow HO_2 + M \quad (R13)$$

Typically, initial concentrations of 1 $\times 10^{16}$ molecule cm^{-3} of O_3 and 0.5–2 $\times 10^{17}$ molecule cm^{-3} of H_2 were used. The generation of OH in this manner also produces HO_2 which further reacts (*e.g.* with O_3) to recycle OH.[27] Simulations of the chemistry indicate an $[HO_2]/[OH]_0$ ratio between 44 and 1900 depending on the initial H_2 and O_3 concentrations (see SI for further details). The use of H_2O_2 and HNO_3 as OH precursors was not possible in the relative-rate method as their rate coefficients for reaction with OH are much larger than for CF_3CHO. In addition, neither O_3 nor H_2 has strong absorption features in the relevant IR regions, which facilitates the analysis of the spectra. The initial concentrations of CF_3CHO and C_2H_6 were typically 8.5 $\times 10^{13}$ molecule cm^{-3} and 1.6 $\times 10^{14}$ molecule cm^{-3}, respectively. As CF_3CHO absorbs dissociatively at 253.65 nm ($\sigma \sim 5 \times 10^{-21}$ cm^2 molecule^{-1}), its slow loss due to photolysis needs to be taken into account for the relative-rate analysis.[3,31] The first-order loss rate constant for CF_3CHO in this set-up (k_{phot})

was obtained by measuring its depletion in the chamber in different bath gases (N_2, N_2/H_2 and synthetic air/H_2) with the photolysis lamps on, but without adding O_3.

2.3. Chemicals

N_2 (Air Liquide, 99.999%) and synthetic air (Air Liquide, 99.999%) were used without further purification. Anhydrous HNO_3 was prepared by mixing H_2SO_4 (Roth, 98%) and KNO_3 (Roth, >99%) and collecting the HNO_3 vapour in a liquid-nitrogen-cooled trap. The liquid HNO_3 was stored at −30 °C. H_2O_2 (AppliChem, 50 wt%) was concentrated by vacuum distillation to >90 wt%. H_2 (Westfalen, 99.999%) was used without further purification. O_3 was photochemically generated from O_2 (Westfalen, 99.999%) and stored on silica gel at −78 °C prior to each experiment. CF_3CHO was prepared by drying the monohydrate (Sigma Aldrich, 75% in water), passing it over P_2O_5 (Thermo Scientific, >99%) and collecting the vapour in a liquid-nitrogen-cooled trap. Diluted samples of gaseous CF_3CHO in N_2 (5–10 wt%) were prepared by manometric methods and stored in a darkened, 20 L glass bulb. C_2H_6 (Air Liquide, 99.95%) was used without further purification.

3. Results & discussion

3.1. Rate coefficients (204–364 K) for k_1 *via* PLP–PLIF

Fig. 1 displays a representative set of OH decays for a range of $[CF_3CHO]$ obtained in N_2 bath gas at 296 K. The IR-absorbance by CF_3CHO for each $[CF_3CHO]$ is shown in the lower panel of this Figure.

The time-dependent OH-LIF signals exhibit strictly mono-exponential behaviour, characterized by their respective decay constants k'. Under pseudo-first-order conditions ($[CF_3CHO] \gg [OH]_0$), the time-dependent OH concentration $[OH]_t$ is given by:

$$[OH]_t = [OH]_0 \times \exp(-k't) \quad (1)$$

where $[OH]_0$ is the initial concentration after the excimer-laser pulse. The first-order decay constant k' includes loss of OH due to reaction with CF_3CHO ($k_1[CF_3CHO]$) as well as reaction with H_2O_2 and diffusive losses. As, for a given experiment, the pressure and temperature diffusive losses are constant and H_2O_2 is unchanged, the latter two terms can be combined as a single term d:

$$k' = k_1[CF_3CHO] + d \quad (2)$$

The rate coefficient k_1 can thus be obtained by plotting k' *versus* $[CF_3CHO]$ as shown in Fig. 2 for experiments conducted at different temperatures. As expected from (1), k' increases linearly with $[CF_3CHO]$. The term d (the y-axis intercept) varied from one experiment to the next according to the temperature, pressure and the H_2O_2 concentration, with its values in the absence of CF_3CHO (not plotted) consistent with those derived from linear fits as shown in Fig. 2. All determinations of k_1 (a total of 17 at various temperatures), obtained using H_2O_2 photolysis as OH source, are listed in Table 1.

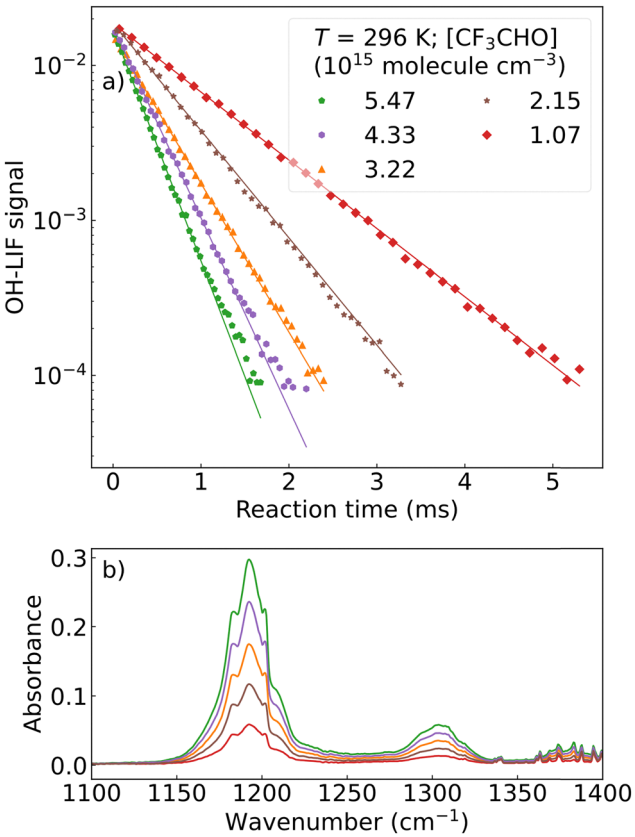

Fig. 1 (a) Exponential decay of the OH-LIF signal over two orders of magnitude *versus* reaction time for five different CF_3CHO concentrations at 296 K. H_2O_2 was used as photolytic OH source. (b) Corresponding FTIR spectra for the five different CF_3CHO concentrations recorded simultaneously with the PLP–PLIF measurements.

As the rate coefficient for OH + CF_3CHO is not large, there is a potential for fast secondary reactions (*i.e.* reaction of OH with radical products) biasing the OH decay constant to high values. As an example, if we assume that CF_3CO radical product of the title reaction reacts with collision frequency ($\sim 2 \times 10^{-10}$ cm^3 molecule^{-1} s^{-1}) with OH to form $CF_3C(O)OH$, then a ~0.1% conversion of CF_3CHO to CF_3CO would result in an enhancement of the OH decay rate (by up to a factor 2 at longer reaction times) and a distortion of the OH decay from mono-exponential behaviour. Such secondary effects can be avoided by working at low initial OH concentrations and thus minimal conversion of CF_3CHO to reactive products. In our experiments the ratio of $[CF_3CHO]/[OH]_0$ was $>1 \times 10^4$ so such effects should be negligible. In order to confirm this, a series of experiments was conducted in which the laser fluence (and thus the initial OH concentration) was varied for a fixed H_2O_2 and CF_3CHO concentration. As shown in Fig. S2.1, k' was independent of the laser fluence and thus independent of $[OH]_0$ over the approximate range 1×10^{10}–5×10^{11} molecule cm^{-3}. This confirms that reactions of OH with products did not influence our rate coefficients and also confirms that radical fragments formed in the photolysis of CF_3CHO did not play a significant role. This is to be expected as the absorption cross-section of

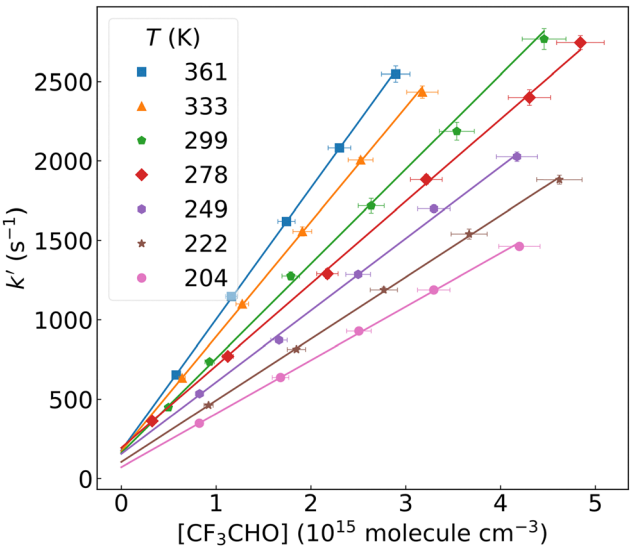

Fig. 2 OH decay constants k' *versus* the concentration of CF_3CHO at different temperatures. The *y*-axis intercept varies from 70 s^{-1} to 190 s^{-1} due to OH loss processes such as the reaction with H_2O_2. The horizontal error-bars combine the 2σ uncertainties obtained from spectral deconvolution, and an estimated systematic uncertainty of 5% related to the IR-cross-section. Uncertainties in the decay constants k' correspond to the 2σ confidence intervals derived from mono-exponential fits to the OH-LIF signals.

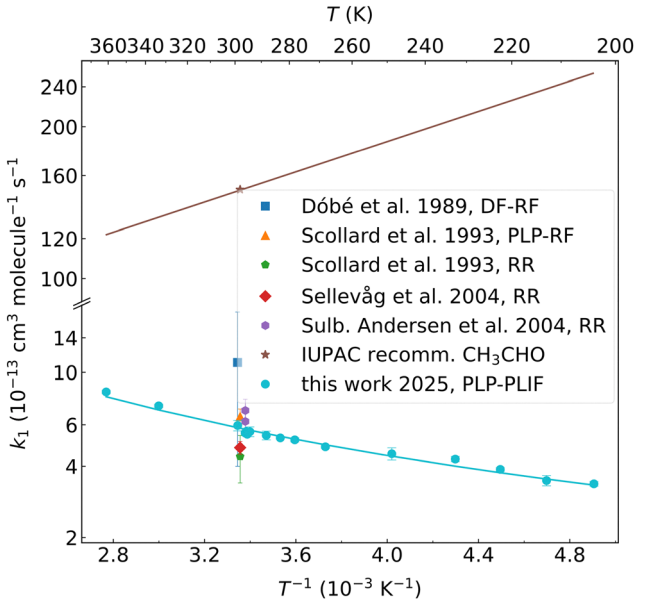

Fig. 3 Temperature dependent rate coefficients from this study (PLP–PLIF) along with literature values.[1–5] Uncertainties in k_1 correspond to the 2σ confidence interval derived from the linear fit of k' *versus* [CF_3CHO]. RR = relative rate method, DF-RF = discharge flow-resonance-fluorescence method.

Table 1 Experimental rate coefficients k_1 obtained using PLP–PLIF

T (K)	p (Torr)	k_1 (10^{-13} cm^3 molecule^{-1} s^{-1})	[CF_3CHO] (10^{15} molecule cm^{-3})
204	103	3.4 ± 0.1	0.8–4.2
213	103	3.5 ± 0.2	1.0–3.8
222	103	3.9 ± 0.1	0.9–4.6
233	103	4.3 ± 0.1	0.8–4.0
244	104	4.0 ± 0.2	0.6–5.5
249	103	4.5 ± 0.3	0.8–4.2
268	96	4.8 ± 0.1	0.4–4.7
278	96	5.2 ± 0.1	0.3–4.8
283	97	5.3 ± 0.1	0.3–5.4
288	97	5.4 ± 0.2	0.3–5.1
294	108	5.6 ± 0.3	1.4–8.0
295	101	5.5 ± 0.1	1.4–5.4
296	107	5.6 ± 0.1	1.1–5.7
296	108	5.5 ± 0.1	1.1–5.5
299	104	6.0 ± 0.3	0.5–4.5
333	106	7.2 ± 0.1	0.6–3.2
361	106	8.3 ± 0.1	0.6–2.9

CF_3CHO at 248 nm (2.60×10^{-21} cm^2 molecule^{-1}) is rather low.[29] The temperature dependent rate coefficients obtained are listed in Table 1 and also plotted in Fig. 3 where an overall positive dependence of k_1 on temperature is observed as well some curvature in the Arrhenius plot. The rate coefficients are well reproduced by the expression:

$$k_1(T) = (3.8 \pm 0.2) \times 10^{-13} \times (T/300)^2 \times \exp[(131 \pm 16)/T] \quad (3)$$

with all data within the 2σ confidence interval. The error bars represent statistical uncertainty only (2σ) as returned by weighted, least-squares fits to the data as shown in Fig. 2 and thus also include statistical uncertainty in deriving concentrations by least-squares fitting of the FTIR spectra to a reference spectrum. A potential source of systematic bias in absolute rate coefficients is related to the measurement of the concentration of the excess reactant, *i.e.* CF_3CHO. In this study, on-line measurement of [CF_3CHO] *via* IR absorption spectroscopy ensures that this parameter is known to better than 5% (see Section 2.1.3). A further potential source of error when measuring relatively low rate coefficients is the presence of reactive impurities which can lead to a positive bias. C_2H_4 is a known impurity in samples of CF_3CHO that reacts with OH ($k = 6.6 \times 10^{-12}$ cm^3 molecule^{-1} s^{-1} at 298 K and 100 Torr N_2).[32,33] C_2H_4 was indeed found as an impurity in our flowing CF_3CHO samples but at concentrations that were $\leq$0.1% of the CF_3CHO concentration. This would bias the result by ~1%, which is much lower than our overall uncertainty and thus negligible.

Our rate coefficient at room temperature is a factor ~270 lower than the value of 1.5×10^{-11} cm^3 molecule^{-1} s^{-1} for the non-fluorinated analogue, CH_3CHO.[5]

$$CH_3CHO + OH \rightarrow CH_3CO + H_2O \quad (R14)$$

The positive dependence of k_1 on temperature also strongly contrasts k_{14}, which decreases with increasing temperature over the same range (*i.e.* from 2.6×10^{-11} at 205 K to ~1.0×10^{-11} at 355 K). As, in both cases, the reaction proceeds *via* abstraction of the aldehydic hydrogen atom, it is clearly the substitution of the CH_3 group by CF_3 that reduces the rate coefficient by reducing the electron density around the carbonyl group. In the case of CH_3CHO, OH is believed to form a pre-reaction complex

(PRC) with a five-membered ring in which the H-atom of OH is attached to the carbonyl oxygen.[34] From the PRC, the reaction may proceed *via* either passing over a barrier to products (*i.e.* a transition state in which the C–H bond lengthens compared to the PRC) or by tunnelling through the barrier, which leads to the observed negative dependence of k(OH + CH_3CHO) on temperature. The lower electron density around the carbonyl group for CF_3CHO results in a much less stable PRC, for which the decomposition back to reactants is faster. This results in a reduced net flux through the transition state to products and thus to a lower rate constant. For CF_3CHO, the contribution of "direct" abstraction (with an associated positive dependence on temperature) becomes relatively more important. The different temperature dependencies observed for CF_3CHO and CH_3CHO may also result from a difference in the barrier heights through the transition states relative to reactants.

3.2. Comparison with literature

The 298 K rate coefficient for the reaction of OH with CF_3CHO from this study is 5.8×10^{-13} cm^3 molecule^{-1} s^1 which can be compared to room-temperature literature values, also plotted in Fig. 3. Our rate coefficient at 298 K agrees well with the IUPAC evaluation of previous datasets for this reaction.[5] This agreement may however be somewhat fortuitous as the previous values cover a range of 1.1×10^{-12} to 4.4×10^{-13} cm^3 molecule^{-1} s^1. The rate coefficient published by Scollard *et al.* was obtained by a similar method to that used here (pulsed laser photolysis to generate OH) and returned a value of k_1 = 6.5×10^{-13} cm^3 molecule^{-1} s^1 which is ~12% larger than our value.[2] We note that Scollard *et al.* did not measure CF_3CHO in-line but relied on manometric measurements (*i.e.* partial pressures and partial flows) which are potential sources of systematic bias, and also do not discuss or rule out the presence of reactive impurities in their CF_3CHO samples (which were only stated to have >99% purity). In addition, the authors state that the initial CF_3CHO/OH ratio was greater than 100, which, given that they used a less sensitive technique for OH detection (resonance fluorescence rather than laser-induced-fluorescence), may not have been sufficient to rule out reactions of OH with secondary products. This in turn would have led to a high bias to their derived rate coefficient as described above. We cannot prove if any of these potential factors may have biased the Scollard *et al.* rate coefficient to slightly higher values than ours, but simply indicate that their slightly larger rate coefficient is consistent with such effects. Scollard *et al.* reported a value for k_1 at room-temperature only, however the same experimental set-up was used to derive rate coefficients between 230 and 355 K, which were only reported as conference proceedings with $k_1 = 3.1 \times 10^{-12} \exp[-(488 \pm 57)/T]$.[35] As these data have not been rigorously peer-reviewed, the IUPAC panel has not considered them in their evaluations.[5] The rate coefficients of Laverdet *et al.*[35] all lie ~10% higher than our values and the same potential reasons as described for Scollard *et al.* apply. In further absolute measurements of k_1, Dóbé *et al.*[1] used a low-pressure flow tube with resonance-fluorescence detection of OH at 299 K. In their experiments the CF_3CHO/OH ratio was between ~50 and 280 which would almost certainly have biased their rate coefficients to high values. Indeed, their rate coefficient is the highest of all literature values (k_1(299 K) = 1.1×10^{-12} cm^3 molecule^{-1} s^1) and was not considered by IUPAC in their evaluation.

In addition to the absolute studies, there are several relative rate experiments which report values of k_1. As in the absolute studies, the values obtained also show considerable scatter (between (6.9 ± 0.1) and $(4.4 \pm 1.0) \times 10^{-13}$ cm^3 molecule^{-1} s^{-1}) depending on the choice of OH-source (RONO photolysis in air or O_3 photolysis in the presence of H_2) and reference reactant including $CH_3C(O)CH_3$ (k_{OH} = 1.8×10^{-13} cm^3 molecule^{-1} s^{-1}), C_2H_6 ($k_{OH} = 2.4 \times 10^{-13}$ cm^3 molecule^{-1} s^{-1}), C_2H_4 ($k_{OH} = 7.8 \times 10^{-12}$ cm^3 molecule^{-1} s^{-1}) and C_2H_2 (k_{OH} = 7.5×10^{-13} cm^3 molecule^{-1} s^{-1}).[5] With the exception of C_2H_4, the other reference reactants all react with rate coefficients which are similar (within a factor of ~two) to that of OH + CF_3CHO and are thus suitable for accurate determination of k_1. The remaining three determinations yield rate coefficients (10^{-13} cm^3 molecule^{-1} s^{-1}) of 4.4 ± 1.0 (Scollard *et al.* 1993), 4.8 ± 0.3 and 5.44 ± 0.71 (Sellevag *et al.* 2004), which are in reasonable agreement.[2,3]

In order to better understand the differences between the various relative rate studies we conducted our own set of experiments in which the relative loss rates of CF_3CHO and C_2H_6 in the presence of an OH-source were determined.

3.3. Relative rate study of OH + CF_3CHO

The relative rate of reaction of OH with CF_3CHO (R1) and C_2H_6 (R15) was measured in the RR-FTIR set-up with the photolysis of O_3 providing the source of OH (R11).

$$C_2H_6 + OH \rightarrow \text{products} \qquad \text{(R15)}$$

As CF_3CHO is lost by both reaction with OH and photolysis the relative change in concentration of CF_3CHO and reference reactant is given by:

$$\ln\left(\frac{[CF_3CHO]_0}{[CF_3CHO]}\right) - J_{phot}t = \frac{k_1}{k_{15}} \times \ln\left(\frac{[C_2H_6]_0}{[C_2H_6]}\right) \qquad (4)$$

where $[CF_3CHO]_0$ and $[C_2H_6]_0$ are initial concentrations of CF_3CHO and C_2H_6, $[CF_3CHO]_t$ and $[C_2H_6]_t$ are the concentrations after reaction time t. k_1 and k_{15} are the bimolecular rate coefficients of the reaction of CF_3CHO and C_2H_6 with OH and J_{phot} is the photolysis frequency of CF_3CHO. $J_{phot} = (8.3 \pm 0.5) \times 10^{-5}$ s^{-1} was determined by monitoring the depletion of CF_3CHO absorption features during the lights-on phase (but in the absence of O_3). More details are provided in the SI (Fig. S4.1).

In the relative-rate experiments, the relative change in concentration of both reactants was monitored *in situ* with FTIR using the infra-red absorption feature at 3030–2957 cm^{-1} for C_2H_6 and three different features of CF_3CHO at 1335–1280 cm^{-1}, 1210–1165 cm^{-1} and 840–860 cm^{-1}. Exemplary FTIR spectra at reaction times of 0, 40 and 170 s are displayed in Fig. 4 along with reference spectra for CF_3CHO and C_2H_6. The strong absorption feature at around 2100 cm^{-1} is from O_3. The spectra were baseline corrected and the absorption

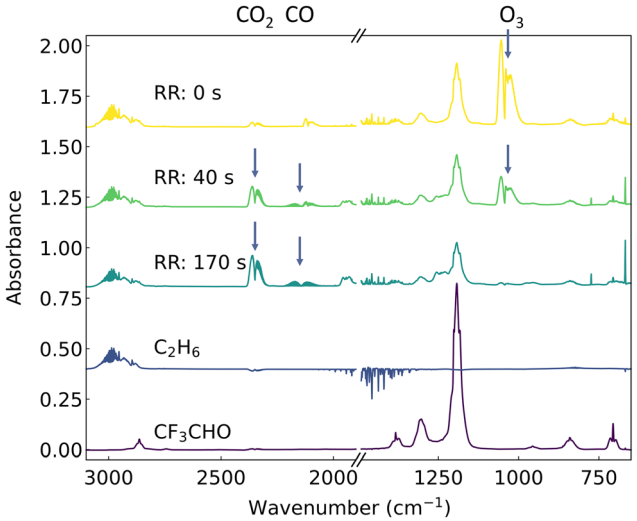

Fig. 4 Plot of the FTIR-spectra measured during a relative-rate experiment at different reaction times (0 s, 40 s and 170 s, upper three traces) along with reference spectra of C_2H_6 and CF_3CHO. The sharp features around 1800 cm^{-1} are due to H_2O vapour. The traces have been vertically offset for clarity of display.

features of H_2O were removed as far as possible by fitting the spectra (2100–1300 cm^{-1}) to a reference spectrum of H_2O. In each composite spectrum, the concentrations of CF_3CHO and C_2H_6 were extracted by orthogonal distance regression to the reference spectra and also the spectra of any overlapping products that could be identified during the experiments. Since all the absorption features used exhibited Beer–Lambert linearity over the concentration range studied (see Fig. S1.2), the ratio of the fitting coefficients is equivalent to the concentration ratio, *i.e.* $[CF_3CHO]_0/[CF_3CHO]_t$ and $[C_2H_6]_0/[C_2H_6]_t$.

As is apparent from Fig. 4, the concentration of O_3 decreases very rapidly, which is related to not only its photolysis but also secondary reactions with H-atoms and both OH and HO_2 radicals (see the SI for more details of the chemical scheme). Both CO_2 and CO (absorption features at ~2350 and 2140 cm^{-1}) are clearly observed products from the degradation of the organic reactants.

Fig. 5 displays the depletion factors for CF_3CHO and C_2H_6, the slope of which gives the relative rate coefficient (k_1/k_{15}) for an experiment conducted with 1.1×10^{16} molecule cm^{-3} of H_2. As discussed previously by Sellevåg *et al.*, H_2 serves two purposes; converting $O(^1D)$ to OH and also scavenging CF_3O in order to prevent it from reacting with either CF_3CHO or C_2H_6.[3]

Values of (k_1/k_{15}) obtained using the relative-rate method range from (1.39 ± 0.03) to (3.06 ± 0.09) depending on the experimental conditions (see Table 2). Using the IUPAC-recommended rate coefficient for OH + C_2H_6 ($k_{15} = 2.4 \times 10^{-13}$ molecule cm^{-3}), the rate coefficient for CF_3CHO + OH varies between (3.3 ± 0.3) to (7.4 ± 0.7) × 10^{-13} cm^3 $molecule^{-1}$ s^{-1}.[5] The variation in the rate coefficient is attributed to (1) the formation of CF_3O radicals and their reaction with CF_3CHO or C_2H_6 when $[H_2]$ is low ((R16) and (R17)) and (2) the removal of CF_3CHO *via* reaction with HO_2 (R18), when $[H_2]$ is high.[36]

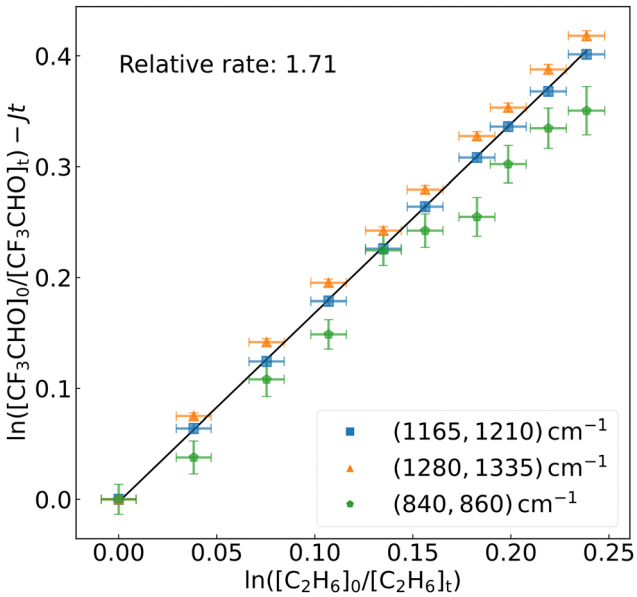

Fig. 5 Depletion factors (logarithmic ratio of initial concentration to concentration at reaction time *t*) for CF_3CHO and C_2H_6 obtained in a relative-rate experiment in N_2 with 1.1×10^{16} molecule cm^{-3} of H_2. The CF_3CHO depletion factor contains the term *Jt* which takes into account its slow loss owing to photolysis. The different colours represent different IR-absorption features that were used to derive the depletion of CF_3CHO and the linear fit (black line) represents an average.

Table 2 Summary of relative rate experiments

Relative rate[a]	Absolute k_1[b] (cm^3 $molecule^{-1}$ s^{-1})	Initial $[H_2]$ (molecule cm^{-3})	Bath gas
1.39 ± 0.03	(3.3 ± 0.3) × 10^{-13}	4.3 × 10^{15}	Air
1.30 ± 0.03	(3.1 ± 0.3) × 10^{-13}	1.1 × 10^{16}	Air
1.71 ± 0.04	(4.1 ± 0.4) × 10^{-13}	1.1 × 10^{16}	N_2
1.95 ± 0.10	(4.7 ± 0.5) × 10^{-13}	1.4 × 10^{17}	Air
3.07 ± 0.09	(7.4 ± 0.7) × 10^{-13}	1.9 × 10^{17}	Air

[a] $k(OH + CF_3CHO)/k(OH + C_2H_6)$. [b] Based on $k(OH + C_2H_6) = 2.4 \times 10^{-13}$ cm^3 $molecule^{-1}$ s^{-1}.

$$CF_3O + CF_3CHO \rightarrow CF_3CO + CF_3OH \quad (R16)$$

$$CF_3O + C_2H_6 \rightarrow C_2H_5 + CF_3OH \quad (R17)$$

$$CF_3O + H_2 (+ O_2) \rightarrow HO_2 + CF_3OH \quad (R18)$$

The source of the CF_3O radicals in these experiments is secondary reactions of CF_3O_2, themselves formed in *e.g.* the self-reaction of the $CF_3C(O)O_2$ radical. The rate coefficient for the reaction of CF_3O with C_2H_6 is 1.3×10^{-12} cm^3 $molecule^{-1}$ s^{-1} but the rate coefficient for CF_3O with CF_3CHO (k_{16}) is not known.[5] The rate coefficient k_{16} was therefore estimated by assuming the same rate coefficient ratio of $k(OH + CF_3CHO)/k(CF_3O + CF_3CHO)$ as that for $k(OH + C_2H_6)/k(CF_3O + C_2H_6)$, resulting in $k_{16} = 3 \times 10^{-12}$ cm^3 $molecule^{-1}$ s^{-1}. In a similar manner, by analogy with the rate coefficients for OH with H_2 and CH_4, the rate coefficient for the reaction of CF_3O with H_2 was estimated to be 2×10^{-12} cm^3 $molecule^{-1}$ s^{-1}. A concentration of H_2 of 2.3×10^{16} molecule cm^{-3}

Table 3 Key reactions considered in the numerical simulations

Reaction	k(298 K) (cm^3 $molecule^{-1}$ s^{-1})
OH reactions	
$OH + CF_3CHO \rightarrow H_2O + CF_3CO$	5.8×10^{-13}
$OH + C_2H_6 \rightarrow H_2O + CH_2CH_3$	2.4×10^{-13} (IUPAC)[5]
Photolysis of TFAA	
$CF_3CHO \rightarrow CF_3 + HCO$	3.28×10^{-5} s^{-1} (IUPAC)[5]
$CF_3CHO \rightarrow CF_3H + CO$	3.04×10^{-5} s^{-1} (IUPAC)[5]
CF_3O reactions:	
$CF_3O + CF_3CHO \rightarrow CF_3OH + CF_3CO$	3.0×10^{-12} (Assumed)
$CF_3O + C_2H_6 \rightarrow CF_3OH + CH_2CH_3$	1.3×10^{-12} (IUPAC)[5]
$CF_3O + H_2 \rightarrow CF_3OH + H$	2.0×10^{-12} (Assumed)
HO_2 reactions	
$HO_2 + CF_3CHO \rightarrow CF_3CH(O)HOO$	2.3×10^{-13} (Long *et al.*, 2022)[36]
$CF_3CH(O)HOO \rightarrow HO_2 + CF_3CHO$	2.0×10^{3} (Long *et al.*, 2022)[36]
$CF_3CH(O)HOO + HO_2 \rightarrow CF_3CH(OH)OOH + O_2$	1.0×10^{-11} (Assumed)

is thus needed to reduce the loss of C_2H_6 and CF_3CHO with CF_3O to <1% of their total (OH-dominated) loss.

To assess the impact of these reactions, we carried out numerical simulations of the chemistry (FACSIMILE[37]) using an assumed reaction scheme (see Table S5.1). The key reactions in the scheme are listed in Table 3. Increasing the H_2 concentration reduces the potential impact of the unwanted reactions of CF_3O with CF_3CHO and C_2H_6 so one would expect the experiments at the highest H_2 concentrations to result in more accurate results. However, the use of very high H_2 also means that not only the CF_3O radical but also a significant fraction of the initially formed OH reacts with H_2 (in air) to form the HO_2 radical ((R19) and (R20)).

$$OH + H_2 \rightarrow H_2O + H \quad (R19)$$

$$H + O_2 + M \rightarrow HO_2 + M \quad (R20)$$

The use of high concentrations of H_2 thus results in a shift in the $[HO_2]/[OH]_0$ ratio towards HO_2 with the simulated ratios varying from 47 at $[H_2] = 10^{16}$ molecule cm^{-3} to 789 at $[H_2] = 2 \times 10^{17}$ molecule cm^{-3} ($[O_3] = 10^{16}$ molecule cm^{-3}). According to a theoretical study,[36] the HO_2 radical may react with CF_3CHO to form the $CF_3CH(OH)OO$ peroxy radical (R21) with a rate coefficient of $k_{20} = 2.34 \times 10^{-13}$ cm^3 $molecule^{-1}$ s^{-1}.

$$CF_3CHO + HO_2 \rightarrow CF_3CH(OH)OO \quad (R21)$$

$$CF_3CH(OH)OO \rightarrow CF_3CHO + HO_2 \quad (R22)$$

$CF_3CH(OH)OO$ is unstable at room temperature and decomposes back to reactants on a ms timescale ($k_{21} = 1.72 \times 10^3$ s^{-1}), which reduces the impact of the reaction between HO_2 with CF_3CHO (R22). However, given the high radical densities in these experiments, some fraction of the $CF_3CH(OH)OO$ radical may react with OH or HO_2 ((R23) and (R24)). This would bias the relative rate coefficient to high values by providing an unwanted, extra sink of CF_3CHO.

$$CF_3CH(OH)OO + OH \rightarrow \text{products} \quad (R23)$$

$$CF_3CH(OH)OO + HO_2 \rightarrow \text{products} \quad (R24)$$

The rate coefficients for (R23) and (R24) are unknown, but a reasonable estimate can be obtained by drawing analogy to other $HO_2 + RO_2$ ($k \sim 1 \times 10^{-11}$ cm^3 $molecule^{-1}$ s^{-1}) and OH + RO_2 reactions ($k \sim 1 \times 10^{-10}$ cm^3 $molecule^{-1}$ s^{-1}).

Using the theoretical rate coefficients from Long *et al.*[36] for the reactions (R20) and (R21) and the estimated rate coefficients for CF_3O with CF_3CHO and H_2, the results of the numerical simulations (see SI for a detailed discussion and Figures) show that, as observed, the relative rate coefficient obtained in the O_3/H_2 photolysis system suffer from systematic bias owing to unwanted reactions of CF_3O with both reactants (when $[H_2]$ is too low) and also reactions of HO_2 with CF_3CHO (when $[H_2]$ is too large). There thus appears to be a narrow window of H_2 concentrations in which these biases in the relative-rate measurements are minimised, and the value obtained approaches that derived from the PLP–PLIF experiments. We conclude that the relative rate studies of this reaction using the OH generation scheme outlined are unlikely to lead to accurate results for k_1. We note that the use of other OH source in relative rate experiments (*e.g.* the photolysis of CH_3ONO/NO mixtures) could conceivably deliver accurate rate coefficients if sufficient NO (or CH_3ONO) is present to scavenge any CF_3O formed and thus prevent its reaction with CF_3CHO or the chosen reference reactant. Such experiments were carried out by Sulbaek-Andersen *et al.* and Scollard *et al.*, though the authors did not consider the possible interfering role of CF_3O.[2,22] In the experiments of Sulbaek-Andersen *et al.*, a large concentration of CH_3ONO was used (a factor 5–10 more than CF_3CHO) which may plausibly have been sufficient to scavenge most CF_3O. In contrast, Scollard *et al.* used almost identical amounts and it is not possible to rule out that some loss of CF_3CHO and/or reference reactant biased their results. The excellent agreement between our PLP–PLIF rate coefficient at room temperature and that obtained by Sulbaek-Andersen *et al.* using the relative-rate technique likely reflects avoidance of potential pitfalls when determining k_1 using absolute and relative methods.

4. Conclusions and atmospheric lifetime of CF_3CHO

We have investigated the reaction between OH and CF_3CHO using PLP–PLIF over an atmospherically relevant temperature range of 204 K to 361 K using a number of OH sources whereby only the photolysis of H_2O_2 generated reproducible, accurate rate coefficients. Our results are summarised by the expression $k_1(T) = (3.8 \pm 0.2) \times 10^{-13} \times (T/300)^2 \times \exp[(131 \pm 16)/T]$ cm^3 $molecule^{-1}$ s^{-1}, reflecting a weak positive dependence on temperature over this temperature range. This is the opposite trend to that observed for the non-fluorinated analogue which, (along with the much lower absolute values of the rate coefficient) is related to destabilisation of the pre-reaction complex by the substitution of H- with F-atoms on the methyl-group. A

series of relative rate experiments revealed sources of potential bias involving formation of the CF_3O radical and its reaction with CF_3CHO and the reference reactant, as well as reactive loss of CF_3CHO through reaction with the HO_2 radical.

For the reasons listed above, we consider our PLP–PLIF experiments, conducted using very high $[CF_3CHO]/[OH]_0$ ratios and also better control of impurities, to be more reliable than the previously published absolute rate studies, which were conducted at room-temperature only. In addition, our room temperature result ($k_1 = (5.8 \pm 0.5) \times 10^{-13}$ cm^3 molecule^{-1} s^{-1}) is in excellent agreement with the previous relative rate study by Sulbaek-Andersen *et al.* ($k_1 = (5.4 \pm 0.7) \times 10^{-13}$ cm^3 molecule^{-1} s^{-1}), which is likely the least affected by secondary reactions involving the CF_3O radical.[22] The tropospheric lifetime of CF_3CHO with respect to OH can be estimated using our temperature dependent rate coefficient and an approximate OH concentration (independent of altitude) of 10^6 molecule cm^{-3}. Based on a standard temperature profile,[38] the lifetime in the lower three kilometres of the troposphere is estimated to be 22 days, increasing to 30 days at altitudes between 8 and 11 kilometres due to the lower temperatures. This is longer than the CF_3CHO lifetime with respect to photolysis, which is presently thought to be <1 week in the boundary layer for which photolysis quantum yields close to room temperature are available.[5]

Conflicts of interest

There are no conflicts to declare.

Data availability

IR characterization of reactants, additional details on the measurements (PLP–PLIF and RR-FTIR), and simulations (reaction scheme) supporting this article are included in the SI. See DOI: https://doi.org/10.1039/d5cp02871j

Acknowledgements

The authors thank AstraZeneca for partial financial support of this investigation. Open Access funding provided by the Max Planck Society.

References

1 S. Dóbé, L. A. Khachatryan and T. Bérces, *Z. Phys. Chem.*, 1989, **93**, 847.
2 D. J. Scollard, J. J. Treacy, H. W. Sidebottom, C. Balestra-Garcia, G. Laverdet, G. Lebras, H. Macleod and S. Teton, *J. Phys. Chem.*, 1993, **97**, 4683.
3 S. R. Sellevåg, T. Kelly, H. Sidebottom and C. J. Nielsen, *Phys. Chem. Chem. Phys.*, 2004, **6**, 1243.
4 M. P. Sulbaek Andersen, C. Stenby, O. J. Nielsen, M. D. Hurley, J. C. Ball, T. J. Wallington, J. W. Martin, D. A. Ellis and S. A. Mabury, *J. Phys. Chem. A*, 2004, **108**, 6325.
5 M. Ammann, R. A. Cox, J. N. Crowley, H. Herrmann, M. E. Jenkin, V. F. McNeill, A. Mellouki, M. J. Rossi, J. Troe and T. J. Wallington, *Evaluated kinetic and photochemical data for atmospheric chemistry*, 2025, https://iupac.aeris-data.fr/.
6 J. C. Boutonnet, P. Bingham, D. Calamari, C. D. Rooij, J. Franklin, T. Kawano, J.-M. Libre, A. McCul-loch, G. Malinverno, J. M. Odom, G. M. Rusch, K. Smythe, I. Sobolev, R. Thompson and J. M. Tiedje, *Hum. Ecol. Risk Assess.*, 1999, **5**, 59.
7 K. R. Solomon, G. J. M. Velders, S. R. Wilson, S. Madronich, J. Longstreth and P. J. Aucamp, *J. Toxicol. Environ. Health, Part B*, 2016, **19**, 289.
8 R. Britton, V. Gouverneur, J.-H. Lin, M. Meanwell, C. Ni, G. Pupo, J.-C. Xiao and J. Hu, *Nat. Rev. Methods Primers*, 2021, **1**, 47.
9 S. Caron, *Org. Process Res. Dev.*, 2020, **24**, 470.
10 Y. Ogawa, E. Tokunaga, O. Kobayashi, K. Hirai and N. Shibata, *iScience*, 2020, **23**, 101467.
11 M. S. Javadi, R. Søndergaard, O. J. Nielsen, M. D. Hurley and T. J. Wallington, *Atmos. Chem. Phys.*, 2008, **8**, 3141.
12 M. D. Hurley, T. J. Wallington, M. P. Sulbaek Andersen, D. A. Ellis, J. W. Martin and S. A. Mabury, *J. Phys. Chem. A*, 2004, **108**, 1973.
13 W. M. O. (WMO), *State of the Global Climate 2022*, Geneva, 2023.
14 J. B. Burkholder, R. A. Cox and A. R. Ravishankara, *Chem. Rev.*, 2015, **115**, 3704.
15 T. J. Wallington, M. P. S. Andersen and O. J. Nielsen, *Adv. Atmos. Chem.*, 2017, **305**, DOI: 10.1142/9789813147355_0005.
16 X. Zhang and Y. Li, *Energy*, 2024, **311**, 133423.
17 A. Tewari, A. Parashar, W. Ahmad, A. Kumar, R. K. Vishwkarma, M. A. Ansari and P. Argulles, *Compressors and Blowers: Maintenance, Practical Guidance, Energy-Efficient Technologies*, 2025, **13**, 179.
18 Y. Wang, Z. Wang, M. Sun, J. Guo and J. Zhang, *Sci. Total Environ.*, 2021, **780**, 146631.
19 M. P. Pérez-Peña, J. A. Fisher, C. Hansen and S. H. Kable, *Environ. Sci.: Atmos.*, 2023, **3**, 1767.
20 M. L. Hanson, S. Madronich, K. Solomon, M. P. Sulbaek Andersen and T. J. Wallington, *Environ. Toxicol. Chem.*, 2024, **43**, 2091.
21 J. Salas, A. L. Cardona, M. A. Burgos Paci and F. E. Malanca, *Atmos. Environ.*, 2024, **337**, 120780.
22 M. P. Sulbaek Andersen, O. J. Nielsen, M. D. Hurley, J. C. Ball, T. J. Wallington, J. E. Stevens, J. W. Martin, D. A. Ellis and S. A. Mabury, *J. Phys. Chem. A*, 2004, **108**, 5189.
23 V. Sivakumaran and J. N. Crowley, *Phys. Chem. Chem. Phys.*, 2003, **5**, 106.
24 M. Wollenhaupt, S. A. Carl, A. Horowitz and J. N. Crowley, *J. Phys. Chem.*, 2000, **104**, 2695.
25 C. B. M. Groß, T. J. Dillon, G. Schuster, J. Lelieveld and J. N. Crowley, *J. Phys. Chem. A*, 2014, **118**, 974.
26 J. N. Crowley, G. Saueressig, P. Bergamaschi, H. Fischer and G. W. Harris, *Chem. Phys. Lett.*, 1999, **303**, 268.
27 M. Berasategui, D. Amedro, A. Edtbauer, J. Williams, J. Lelieveld and J. N. Crowley, *Atmos. Chem. Phys.*, 2020, **20**, 2695.

28 R. Atkinson, D. L. Baulch, R. A. Cox, J. N. Crowley, R. F. Hampson, R. G. Hynes, M. E. Jenkin, M. J. Rossi, J. Troe and T. J. Wallington, *Atmos. Chem. Phys.*, 2008, **8**, 4144.
29 M. S. Chiappero, F. E. Malanca, G. A. Argüello, S. T. Wooldridge, M. D. Hurley, J. C. Ball, T. J. Wallington, R. L. Waterland and R. C. Buck, *J. Phys. Chem. A*, 2006, **110**, 11944.
30 A. J. C. Bunkan, G. Srinivasulu, D. Amedro, L. Vereecken, T. J. Wallington and J. N. Crowley, *Phys. Chem. Chem. Phys.*, 2018, **20**, 11306.
31 Y. Hashikawa, M. Kawasaki, R. L. Waterland, M. D. Hurley, J. C. Ball, T. J. Wallington, M. P. S. Andersen and O. J. Nielsen, *J. Fluorine Chem.*, 2004, **125**, 1925.
32 R. Atkinson, D. L. Baulch, R. A. Cox, J. N. Crowley, R. F. Hampson, R. G. Hynes, M. E. Jenkin, M. J. Rossi and J. Troe, *Atmos. Chem. Phys.*, 2006, 3625, DOI: **10.5194/acp-6-3625-2006**.
33 M. P. Sulbaek Andersen, M. D. Hurley, T. J. Wallington, J. C. Ball, J. W. Martin, D. A. Ellis, S. A. Mabury and O. J. Nielsen, *Chem. Phys. Lett.*, 2003, **379**, 28.
34 I. W. M. Smith and A. R. Ravishankara, *J. Phys. Chem. A*, 2002, **106**, 4798.
35 G. Laverdet, G. Le Bras, H. MacLeod, G. Poulet, S. Teton, D. Scollard, J. Treacy and H. Sidebottom, *Laser photolysis-resonance fluorescence investigation of the reactions of hydroxyl radicals with CCl3CHO and CF3CHO as a function of temperature*, SPIE, 1993.
36 B. Long, Y. Xia and D. G. Truhlar, *J. Am. Chem. Soc.*, 2022, **144**, 19910.
37 A. R. Curtis and W. P. Sweetenham, *Facsimile, Atomic Energy Research Establishment, Report R-12805*, 1987.
38 U. S. Atmosphere, *US standard atmosphere*, National Oceanic and Atmospheric Administration, 1976.

